JOM, Vol. 69, No. 4, 2017
DOI: 10.1007/s11837-016-2252-z

Sintering Behavior and Microstructure Formation of Titanium Aluminide Alloys Processed by Metal Injection Molding

JULIANO SOYAMA,[1,2,3] MICHAEL OEHRING,[1] THOMAS EBEL,[1] KARL ULRICH KAINER,[1] and FLORIAN PYCZAK[1]

1.—Institute of Materials Research, Helmholtz-Zentrum Geesthacht, Max-Planck-Straße 1, 21502 Geesthacht, Germany. 2.—Departamento de Engenharia de Materiais (DEMa), Universidade Federal de São Carlos, Rodovia Washington Luís, km 235, São Carlos 13565-905, Brazil. 3.—e-mail: julianosoyama@gmail.com

The sintering behavior of metal injection molded titanium aluminide alloys, their microstructure formation and resulting mechanical properties were investigated. As reference material, the alloy Ti-45Al-5Nb-0.2B-0.2C at.% (TNB-V5) was selected. Additionally, two other variations with Mo and Mo + Si additions were prepared: Ti-45Al-3Nb-1Mo-0.2B-0.2C at.% and Ti-45Al-3Nb-1Mo-1Si-0.2B-0.2C at.%. The results indicate that the optimum sintering temperature was slightly above the solidus line. With proper sintering parameters, very low porosities ($<0.5\%$) and fine microstructures with a colony size <85 μm could be achieved. Considering the sintering temperatures applied, the phase transformations upon cooling could be described as $L + \beta \rightarrow \beta \rightarrow \alpha + \beta \rightarrow \alpha \rightarrow \alpha + \gamma \rightarrow \alpha_2 + \gamma$, which was in agreement with the microstructures observed. The effects of Mo and Si were opposite regarding the sintering behavior. Mo addition led to an increase in the optimum sintering temperature, whereas Si caused a significant decrease.

INTRODUCTION

Titanium aluminides are lightweight intermetallics that show excellent creep resistance.[1,2] Consequently, their application as high-temperature materials offers great potential for decreasing fuel consumption and simultaneously improving performance.[3] Applications vary from the conservative aircraft industry[4] to cost-oriented automobile manufacturers.[5,6] The fabrication of titanium aluminides is nonetheless challenging considering their brittleness and sensitivity to chemical composition (phase balance is considerably influenced by only slight compositional changes).[7] Therefore, near-net shape powder metallurgy techniques are attractive processing methods because they offer good control of chemical composition and lead to fine and homogenous microstructures, as well as to the avoidance of extensive machining.[8]

The majority of powder metallurgy techniques require sintering for the final consolidation of the part. The sintering step including the cooling process is critical because it controls microstructure formation and can be a source of defects and dimensional distortions. Furthermore, the sintering behavior is heavily dependent on the metallic powders.[9] For instance, pre-alloyed powders sinter differently in comparison to a mixture of elemental powders.[10,11] Therefore, in any powder metallurgy technique, the characteristics of the powders determine not only the shaping process parameters but also the sintering behavior.

Typical sintering temperatures of titanium aluminides are very high (about 1500°C).[12,13] When compared to more traditional materials, for instance, steels, high sintering temperatures necessitate the use of powerful and accordingly expensive furnaces. Therefore, different approaches have been investigated to decrease the sintering temperature in order to reduce costs of both equipment and processing. It is possible to decrease the solidus line, for instance by the addition of Zr,[12] or by adding elements that cause transient liquid phase formation during sintering, which decreases residual porosity.[14,15] Obviously, by changing the chemical composition, different phase formation and microstructure evolution take place. Since lowering the sintering temperature might decrease

(Published online January 12, 2017)

the high-temperature mechanical strength, it is important to find a compromise between the two properties.

In this work, different alloy compositions were investigated in regard to sintering behavior, microstructure formation, and mechanical properties. TNB-V5 (Ti-45Al-5Nb-0.2B-0.2C at.%) was selected as reference material due to its balanced mechanical properties and excellent creep resistance.[16] The objective of varying the composition was twofold: firstly, to study the sintering behavior of these compositions that up to now have not been reported, and secondly, to improve the mechanical properties. The elements selected for these purposes were Si and Mo. Si leads to the formation of hard particles (silicides),[17] while Mo effects solid solution hardening, but, depending on the heat treatment, also precipitation hardening with B2 particles.[18] However, since Mo is a strong β phase stabilizer, its content must be cautiously selected in order to avoid extensive β phase formation that might be harmful to the mechanical properties. Moreover, due to its high melting point, additions of Mo bear the risk of increasing the sintering temperature. The specimen preparation was carried out by metal injection molding (MIM) and sintering was conducted at different temperatures, depending on the composition. An indication of the sintering temperatures was obtained by differential scanning calorimetry (DSC). Lastly, the microstructure formation in sintered MIM specimens has been described and the resulting mechanical properties at room temperature evaluated.

EXPERIMENTAL PROCEDURE

Ingots with the composition Ti-45Al-5Nb-0.2B-0.2C and Ti-45Al-3Nb-1Mo-0.2B-0.2C (all compositions mentioned in the text are in at.%) supplied by GfE, Nürnberg, Germany, were used as raw material for the preparation of pre-alloyed powders. The ingots were gas-atomized with argon at Helmholtz-Zentrum Geesthacht, Germany. Only the fraction <45 μm was used to prepare the specimens. The oxygen levels of the atomised powders measured by a melt extraction technique were 845 μg/g oxygen for Ti-45Al-5Nb-0.2B-0.2C and 708 μg/g for Ti-45Al-3Nb-1Mo-0.2B-0.2C. Three compositions were prepared from each of the pre-alloyed powders: Ti-45Al-5Nb-0.2B-0.2C (reference material), Ti-45Al-3Nb-1Mo-0.2B-0.2C and Ti-45Al-3Nb-1Mo-1Si-0.2B-0.2C, hereafter called TNB-V5, 3Nb-1Mo and 3Nb-1Mo-1Si, respectively.

The specimens were prepared by MIM using an Arburg machine, Allrounder 320S, with the geometry of tensile specimens according to ISO 2740. The feedstock was prepared under argon atmosphere by mixing the metallic powder and binder system (10 wt.%) in a double Z-Blade mixer (Femix KM, 0.5 K) for 2 h at 120°C. The binder system consisted of paraffin waxes, polyethylene-vinyl-acetate and stearic acid and was applied at a fraction of 10 wt.% (about 32 vol.%). This binder content was selected because it leads to adequate feedstock viscosity for the MIM process and a better surface quality in the sintered parts.[19] The addition of Si powder (Alfa Aesar, 99.5% with particle size <45 μm) was conducted during feedstock preparation. After MIM, the paraffin waxes were removed chemically in a bath of hexane for 15 h at 45°C, and the remaining binder was removed thermally. The thermal debinding and sintering were carried out in a single furnace run using a cold wall furnace from XERION, Germany, of the XVAC series. Sintering was conducted in high vacuum of approximately 10^{-4} mbar at different temperatures, depending on the composition, for 2 h. The oxygen and carbon levels were measured in the sintered specimens by means of a melt extraction technique (LECO System). The model TC-436AR was used for oxygen, while the CS-444 was used for carbon analysis.

For microstructural investigation, the sintered specimens were mounted in resin followed by grinding and polishing procedures. An Olympus PMG-3 light microscope together with the image analysis software AnalySIS pro was used for porosity and colony size measurements. The linear intercept method was applied to determine the colony size. Backscattered electron images were recorded using a scanning electron microscope (DSM962; Zeiss). The powders were analysed by DSC under argon for the investigation of the sintering behavior. The DSC experiments were conducted in a Netzsch DSC404 Pegasus calorimeter using a heating rate of 20 K/min. Density measurements were carried out by the immersion method (ASTM B311) using an analytical scale, Sartorius LA230S.

The tensile tests were conducted using specimens with a strain gauge of 30 mm at room temperature. A servohydraulic test machine model MTS 810 from Materials Testing Systems with a load cell of 100 kN capacity was used. The strain rate applied was 2.38×10^{-5}/s. The elongation was measured by an extensometer attached to the ridges of the specimen. Three specimens were tensile tested and the results averaged.

RESULTS AND DISCUSSION

Sintering Behavior

The sintering behavior was investigated by DSC, which served as a guide for finding appropriate sintering temperatures, and by conducting various sintering cycles at different temperatures. Figure 1 shows the DSC curve for TNB-V5 measured during heating. The several phase transformations that occur up to the melting point are indicated. Two important points were the β-transus that indicates the lowest temperature where the β phase is stable and the onset of the melting peak where the liquid phase becomes stable (solidus line). Considering that diffusion is faster in the β phase,[20] the β-

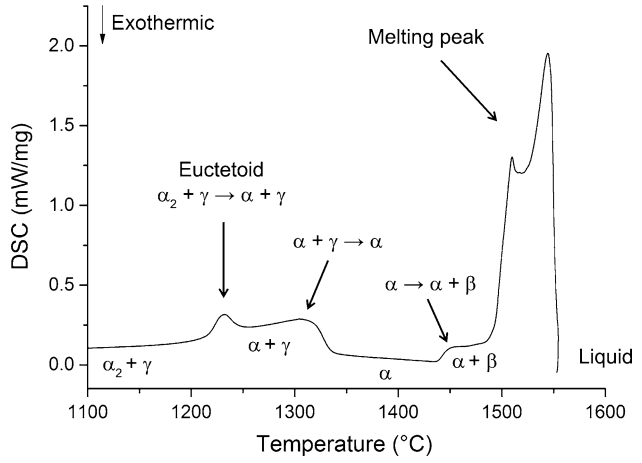

Fig. 1. DSC curve during heating of TNB-V5 at 20 K/min.

transus temperature is an interesting lower boundary for sintering, whereas the limiting upper temperature is dictated by the melting peak.

Sintering experiments were conducted with the reference material (TNB-V5) at various temperatures ranging from the β-transus temperature up to above the solidus line. The results are shown in Table I. Clearly, sintering conducted completely in the solid state led to low porosity (in the order of 1% at 1480°C/2 h). However, extremely low porosities ($<0.3\%$) were possible only with sintering temperatures slightly above the onset of the melting peak in a near-solidus sintering condition. Higher sintering temperatures (>1510°C) led to the formation of pronounced liquid phase fractions that caused dimensional distortion. In contrast to the elemental powder metallurgy approach, the use of pre-alloyed powders leads to lower porosities because the exothermic reactions between Ti and Al cause swelling and Kirkendall porosity does not take place.[11] The lower density and heterogeneous microstructures[21] due to the reactive sintering reactions are the major drawback for powder metallurgy-processed titanium aluminides, but they can be completely mitigated by using pre-alloyed powders. However, pre-alloyed powders are harder, and thus more difficult to shape by uniaxial pressing, requiring >1.2 GPa to achieve an acceptable green strength.[22] Consequently, MIM offers a good compromise of processability, sintered density and microstructural homogeneity.

Like any sintered material, MIM-processed titanium aluminides are believed to undergo all three stages of sintering. Firstly, the powder particles come together forming necks, then the necks grow, and finally the part becomes dense with little residual porosity left. The major densification mechanisms are dependent on liquid phase and diffusion (grain boundary, surface and volume) rather than evaporation/condensation, since the sintering atmosphere applied was a vacuum. Simultaneously with the heating and cooling stages of the sintering process, the various solid-state transformations described in the binary phase diagram take place, which can critically affect the sintered microstructure.

Even though the precise discrimination between each stage of sintering is difficult, it can be concluded that temperatures as high as 1300°C are necessary to achieve the intermediate stage in the case of TNB-V5.[7] Nevertheless, heavy diffusing elements such as Mo, Zr, W, Ta, etc. might delay neck formation. The analysis of the sintered densities in Table I shows that the porosity changes from 8.9% to 3.3% for specimens sintered at 1460°C and 1470°C. Typically, a change in the pore structure from smooth interconnected to isolated occurs at porosities in the order of 5%, which characterises the start of final stage sintering. Consequently, at temperatures around 1460°C, the final stage sintering is reached. Table I additionally shows that little change in the porosity of TNB-V5 takes place between 1490°C and 1510°C. In fact, the mechanical properties of TNB-V5 sintered at 1490°C would probably suffice for many load-bearing applications. Nonetheless, for applications in which the shape of the pores are important, e.g., fatigue or thermal fatigue, higher sintering temperatures are necessary to achieve rounder pores.[12]

Based on the findings that near-solidus sintering in the case of TNB-V5 is more efficient to achieve very low porosity, the sintering temperatures for the alloy variations were selected by determining their melting peaks through DSC analysis, as shown in Table II. The addition of Mo decreased the β-transus temperature by about 45°C in comparison to TNB-V5. Moreover, Mo induced an increase in the onset of the melting peak, which in turn is reflected in increasing the optimum sintering temperature. On the other hand, additions of Si led to a significant decrease (35°C) in the onset of the melting peak. Independent of the alloy variation, with proper selection of the near-solidus sintering temperature, very low porosities ($<0.2\%$) could be achieved. With additions of Mo and Mo + Si, a pronounced decrease in the colony size also took place. In the case of Mo + Si addition, the colonies were half the size of the reference material.

The effects of adding Mo and Si were opposite in regard to optimum sintering temperatures. Mo has a high melting point and is a strong β-stabilizing element. Therefore, the change in the β-transus temperature, as well as the slight increase in the solidus line, was expected. In addition, Mo is a heavy diffusing atom and it thus hampers mass transport and densification during sintering. Considering that near-solidus sintering temperatures were applied, with an increase in the solidus line, an increase in the optimum sintering temperatures naturally followed. In contrast, with Si addition, the onset of the melting peak was considerably shifted to lower temperatures. Therefore, the specimen 3Nb-1Mo-1Si could be sintered in a near-solidus

condition at a much lower temperature. A possible explanation for the decreased sintering temperature in the case of Si addition could be due to the formation of a transient liquid phase before the formation of silicides. However, apart from the shift in the melting peak, no evidence of a different phase transformation at high temperatures could be observed in in the DSC curves. Despite the lower onset of the melting peak due to Mo addition, 3Nb-1Mo-1Si still showed a β-transus temperature similar to 3Nb-1Mo. Consequently, the shift in the melting peak is likely a thermodynamic effect rather than kinetic and does not involve a transient liquid phase.

Microstructure Formation

The scanning electron microscopy (SEM) micrographs of the sintered specimens are shown in Fig. 2. All microstructures were fully lamellar and shared some common features such as pores and boride particles. In the case of TNB-V5, a local enrichment of heavy elements (Nb) was also identified (Fig. 2a). In 3Nb-1Mo and 3Nb-1Mo-1Si, these regions were composed of Nb and Mo. Additionally, the β phase could also be found at grain boundary triple points in the specimens containing Mo. The phase fraction was, however, small. For the 3Nb-1Mo-1Si, fine particles that are most probably titanium silicides (Ti_5Si_3), were additionally identified (Fig. 2d).

The sintered microstructures of the alloys investigated were all fully lamellar. The sintering temperatures were in the range of the β + L phase field and consequently passing through the α phase field while cooling took place. The lamellar structure forms as the $\alpha + \gamma$ phase field is crossed, which happens progressively with the γ phase precipitating from the α phase. Further cooling leads to the ordering of the hexagonal α phase, changing it to the α_2 phase. Considering that the most appropriate sintering temperatures for achieving very low porosity were slightly above the solidus line, the phase transformations during cooling from the sintering temperature can be described as: $L + \beta \rightarrow \beta \rightarrow \alpha + \beta \rightarrow \alpha \rightarrow \alpha + \gamma \rightarrow \alpha_2 + \gamma$. In the case of Mo addition (β stabilizer), the phase formation during cooling can be modified to include the presence of a stabilized β phase (β_s): $L + \beta \rightarrow \beta \rightarrow \alpha + \beta \rightarrow \alpha + \beta_s \rightarrow \alpha + \gamma + \beta_s \rightarrow \alpha_2 + \gamma + \beta_s$. The major microstructural differences between TNB-V5 and the alloy variations tested were the presence of the stabilized β phase and of titanium silicides, which were also formed upon cooling from the sintering temperature. Another important phenomenon is the formation of Nb microsegregations (also including Mo for 3Nb-1Mo and 3Nb-1Mo-1Si), which appeared as a network with bright contrast in BSE pictures. These regions arise due to the $\beta \rightarrow \alpha$ phase transition, when the β-stabilizing elements are rejected for the β phase and remain at the former α/β phase boundaries. In the case of 3Nb-1Mo and 3Nb-1Mo-1Si, the enrichment of β-stabilizing elements caused the β phase to be stabilized at room temperature, remaining mostly at the colony boundaries and triple points.

The refinement of colony size observed with Mo and Mo + Si additions can be explained by the effect of more heterogeneous nucleation sites for the α phase and hindering of grain growth in the single α phase field during cooling. Both effects depend on the presence of an additional phase (borides and Ti_5Si_3) while the transformation $\beta \rightarrow \alpha + \beta \rightarrow \alpha$ takes place. Therefore, by adding Mo and Mo + Si, it was possible not only to change the optimum sintering temperatures but also to refine the microstructure due to the different phase transformations upon cooling from the sintering temperature.

Table I. Sintering behaviour of TNB-V5. The sintering time was 2 h

Sintering temperature (°C)	Porosity (%)	Sintered density (g/cm^3)
1460	8.9 ± 0.6	3.81
1470	3.3 ± 0.3	3.93
1480	1.1 ± 0.1	4.06
1490	0.24 ± 0.04	4.12
1500	0.13 ± 0.1	4.13
1510	0.15 ± 0.04	4.12

Mechanical Properties

The tensile properties of the alloys investigated are displayed in Table III. The alloy 3Nb-1Mo-1Si showed the highest ultimate tensile stress, while

Table II. β-transus temperatures, the onset of melting peaks, actual sintering temperature applied, residual porosity and colony size of the alloys investigated

Composition	$\alpha \rightarrow a + b$ (°C)	Onset of melting peak (°C)	Sintering temperature (°C)	Porosity (%)	Colony size (μm)
TNB-V5	1438	1497	1500	0.13 ± 0.1	82 ± 3
3Nb-1Mo	1393	1502	1510	0.08 ± 0.05	62 ± 6
3Nb-1Mo-1Si	1392	1462	1470	0.13 ± 0.09	42 ± 4

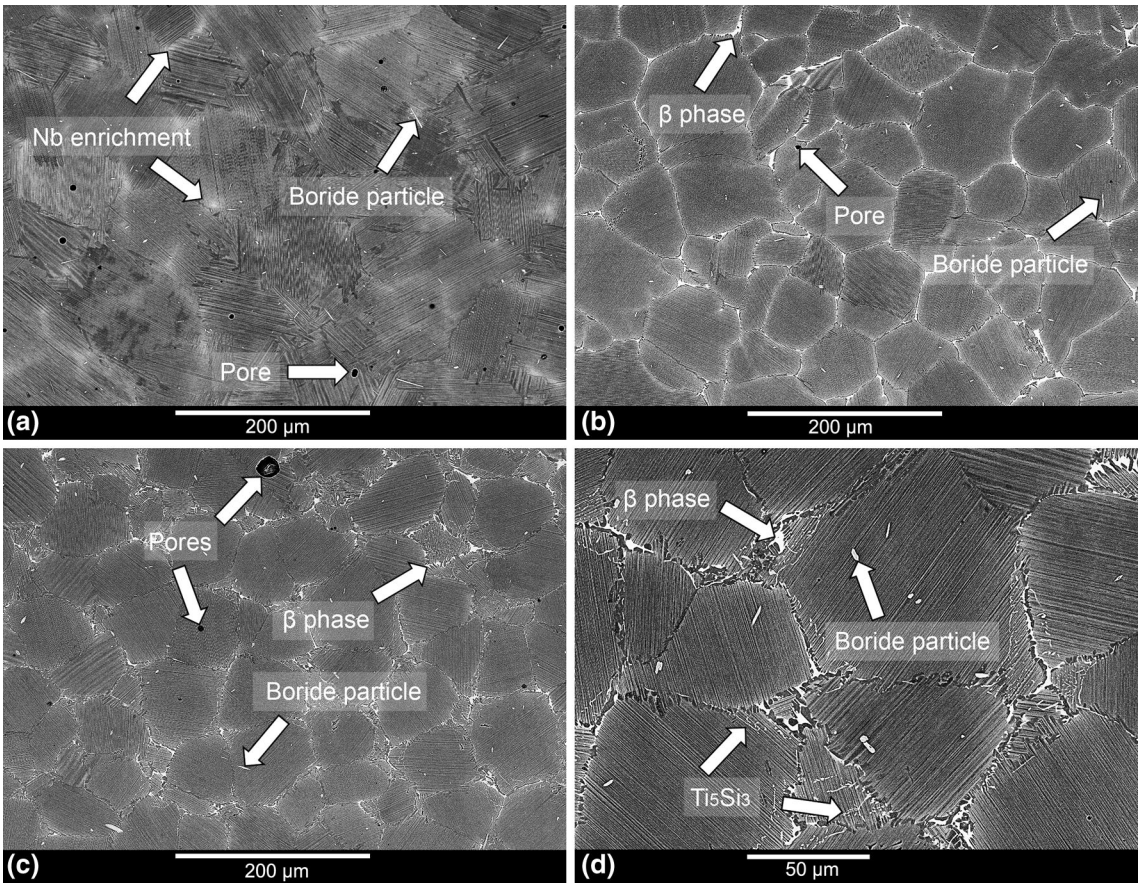

Fig. 2. SEM micrographs of sintered specimens. (a) TNB-V5, (b) Nb-1Mo, (c) 3Nb-1Mo-1Si, (d) 3Nb-1Mo-1Si, detail of β phase at grain boundary triple points and Ti_5Si_3.

TNB-V5 and 3Nb-1Mo displayed overlapping error bars. TNB-V5 showed slightly more plastic deformation. However, the strain at fracture was the same for all alloys.

Figure 3 shows three representative uniaxial tensile stress–strain curves. The small improvements in the ultimate tensile strength (UTS) with 3Nb-1Mo and 3Nb-1Mo-1Si in comparison to TNB-V5 are indicated. Despite the change in composition, the elastic behavior was quite similar.

Kim et al.[23] showed that there is a direct relationship between colony sizes, tensile strength and ductility for titanium aluminides. The Hall–Petch relationship has also been demonstrated to be valid for a wide variety of titanium aluminides.[2] Naturally, as the colonies get smaller, the more difficult it becomes for the dislocations to move. Nonetheless, the Hall–Petch relationship is questionable in the case of fully lamellar microstructures because the lamellar spacing also plays an important role. Consequently, the higher UTS of 3Nb-1Mo-1Si can only be partly explained by the finer colony size. Since the specimens were cooled at the same rate after sintering, the lamellar spacing is assumed to be constant. Consequently, an additional contribution to the improved tensile properties is probably

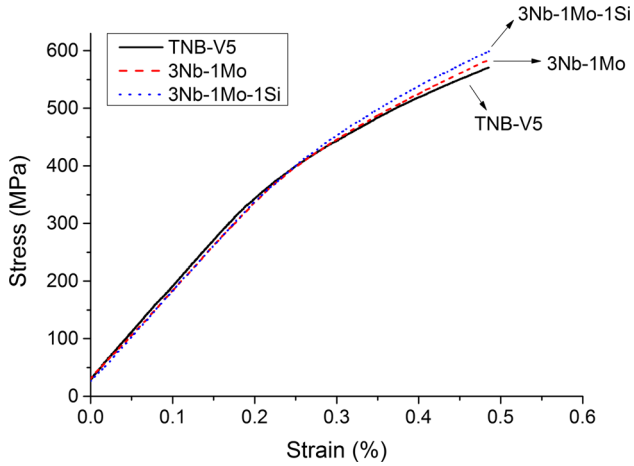

Fig. 3. Representative tensile stress–strain curves at room temperature.

from precipitation strengthening, which was the main difference between 3Nb-1Mo and 3Nb-1Mo-1Si. In comparison to duplex microstructures of extruded high Nb containing titanium aluminides that can achieve UTS >1000 MPa and yet considerable ductilities of 1–2%,[16] the room-temperature

Table III. Tensile properties of the alloys investigated at room temperature

Alloy	UTS (MPa)	Plastic strain (%)	Strain at fracture (%)
TNB-V5	570 ± 1	0.12 ± 0.01	0.5 ± 0.01
3Nb-1Mo	571 ± 17	0.10 ± 0.03	0.5 ± 0.01
3Nb-1Mo-1Si	607 ± 10	0.08 ± 0.02	0.5 ± 0.0

Table IV. Oxygen and carbon levels measured in the alloys investigated after sintering

Alloy	Oxygen (μg/g)	Carbon (μg/g)
TNB-V5	1780 ± 28	751 ± 87
3Nb-1Mo	1555 ± 42	1192 ± 8
3Nb-1Mo-1Si	1536 ± 53	1237 ± 64

tensile properties of MIM-TiAl alloys are rather unsatisfactory. Nonetheless, when compared to the cast + HIP conditions of similar compositions, the mechanical properties are within the same range. For instance, Ti-46Al-8Nb was reported to show UTS of 482 MPa and 0.2% elongation,[24] while the same alloy with a refined microstructure due to boron addition, Ti-46Al-8Nb-1B, showed 620 MPa and 0.8%.[25] Obviously, the levels of oxygen and carbon and the microstructures of the cast + HIP materials are different from materials processed by MIM; however, considering that MIM is a near-net shape process, the as-sintered tensile properties are quite acceptable.

The oxygen and carbon levels of the sintered specimens are shown in Table IV. The reference material showed the highest oxygen content but the lowest carbon content. 3Nb-1Mo and 3Nb-1Mo-1Si showed similar values for both oxygen and carbon. The carbon contents are difficult to control in MIM due to the presence of the organic binder required for shaping, thus producing the scatter found among the different alloys. The pick-up of impurities is inevitable in any powder metallurgy processing technique. Before the finished consolidated part is achieved, several steps involving powder handling are necessary, which usually contribute to increased levels of oxygen, carbon and nitrogen, in addition to the impurities already present in the starting powders. If the solubility limit of interstitial elements is exceeded, precipitation of oxides, carbides and nitrides takes place.[16] The starting carbon value (0.2 at.%) accounts for 600 μg/g, therefore it is clear that carbon pick-up occurred during the process. Moreover, the pre-alloyed powders contained approximately 700–800 μg/g of oxygen, consequently their levels practically doubled in the sintered specimens, which could explain the small plasticity of MIM-processed alloys.

Elements such as oxygen and carbon can significantly influence the mechanical properties either due to solid solutions or through the formation of precipitates. Solely by analyzing their levels in Table IV, it is not possible to discriminate their individual contribution to the mechanical properties. However, since their presence usually involves an increase in tensile and creep resistance, it is reasonable to assume that their effect in the alloys studied was not completely detrimental.

CONCLUSION

The sintering behavior and microstructure formation of titanium aluminides prepared by metal injection molding were investigated. The most suitable sintering temperatures were slightly above the solidus line leading to very low porosity (<0.2%). The effects of Mo and Si on the optimum sintering temperature were opposite. While Mo addition increased the optimum sintering temperature, Si addition significantly decreased it, which was a result of a shift in the solidus line. Furthermore, the changes in chemical composition led to the formation of a stabilized β phase and the precipitation of fine particles (titanium silicides, Ti_5Si_3) which contributed to a refinement of colony size and improved the tensile strength at room temperature.

ACKNOWLEDGEMENTS

The authors would like to thank Andreas Dobernowsky, Dr. Dapeng Zhao, Dirk Matthiessen, Dr. Frank-Peter Schimansky, Gert Wiese, Dr. Jonathan Paul, Prof. Dr. Michael Dahms, Petra Fischer, Uwe Lorenz, Dr. Victor Vitusevych and Wolfgang Limberg.

REFERENCES

1. Y.-W. Kim, *JOM* 47, 38 (1995).
2. F. Appel, J.D.H. Paul, and M. Oehring, *Gamma Titanium Aluminide Alloys: Science and Technology*, 1st ed. (Weinheim: Wiley-VCH Verlag, 2011).
3. Y.W. Kim, *JOM* 47, 39 (1995).
4. P. Bartolotta, J. Barrett, T. Kelly, and R. Smashey, *JOM* 49, 48 (1997).
5. A.K. Sachdev, K. Kulkarni, Z.Z. Fang, R. Yang, and V. Girshov, *JOM* 64, 553 (2012).
6. M.M. Keller, P.E. Jones, W.J. Porter, and D. Eylon, *JOM* 49, 42 (1997).
7. J. Soyama, M. Oehring, W. Limberg, T. Ebel, K.U. Kainer, and F. Pyczak, *Powder Metall.* 58, 369 (2016).
8. M. Scharvogel and W. Winkelmueller, *JOM* 63, 94 (2011).
9. B. Liu and Y. Liu, *Titanium Powder Metallurgy*, 1st ed., ed. M. Qian and F.H. Froes (Waltham: Elsevier, 2015), pp. 515–531.
10. S. Ma, J. Xing, G. Liu, D. Yi, H. Fu, J. Zhang, and Y. Li, *Mater. Sci. Eng., A* 527, 6800 (2010).
11. S. Ye, H. Hao, W. Mo, K. Yu, L. Liu, C. Deng, and P. Yu, *J. Alloys Compd.* 673, 399 (2016).
12. J. Soyama, M. Oehring, W. Limberg, T. Ebel, K.U. Kainer, and F. Pyczak, *Mater. Des.* 84, 87 (2015).
13. W. Limberg, T. Ebel, F. Pyczak, M. Oehring, and F.P. Schimansky, *Mater. Sci. Eng., A* 552, 323 (2012).
14. Y. Xia, G.B. Schaffer, and M. Qian, *J. Alloys Compd.* 578, 195 (2013).

15. Y. Xia, P. Yu, G.B. Schaffer, and M. Qian, *Mater. Sci. Eng., A* 574, 176 (2013).
16. F. Appel, M. Oehring, and R. Wagner, *Intermetallics* 8, 1283 (2000).
17. T. Klein, B. Rashkova, D. Holec, H. Clemens, and S. Mayer, *Acta Mater.* 110, 236 (2016).
18. M. Takeyama and S. Kobayashi, *Intermetallics* 13, 993 (2005).
19. O.M. Ferri, T. Ebel, and R. Bormann, *Mater. Sci. Eng., A* 527, 1800 (2010).
20. Y. Mishin and C. Herzig, *Acta Mater.* 48, 589 (2000).
21. J. Soyama, M. Oehring, W. Limberg, T. Ebel, K.U. Kainer, and F. Pyczak, *Powder Metall.* 58, 5 (2015).
22. A.A. Zaitsev, Y.Y. Kaplanskii, Z.A. Sentyurina, E.A. Levashov, A.V. Kasimtsev, Y.S. Pogozhev, S.N. Yudin, T.A. Sviridova, and A.V. Malyarov, *Russ. J. Non-Ferrous Met.* 57, 113 (2016).
23. Y.-W. Kim, *Mater. Sci. Eng., A* 192–193, 519 (1995).
24. D. Hu, X. Wu, and M.H. Loretto, *Intermetallics* 13, 914 (2005).
25. D. Hu, J.F. Mei, M. Wickins, and R.A. Harding, *Scr. Mater.* 47, 273 (2002).